

PART OF A SPECIAL ISSUE ON FUNCTIONAL–STRUCTURAL PLANT MODELLING

Modelling reveals endogenous osmotic adaptation of storage tissue water potential as an important driver determining different stem diameter variation patterns in the mangrove species *Avicennia marina* and *Rhizophora stylosa*

Maurits W. Vandegehuchte^{1,*}, Adrien Guyot², Michiel Hubeau¹, Tom De Swaef³, David A. Lockington² and Kathy Steppe¹

¹Laboratory of Plant Ecology, Faculty of Bioscience Engineering, Ghent University, Coupure links 653, 9000 Gent, Belgium, ²National Centre for Groundwater Research and Training School of Civil Engineering, The University of Queensland, 4072 Brisbane, Australia and ³Plant Sciences Unit, Institute for Agricultural and Fisheries Research (ILVO), Caritasstraat 21, 9090 Melle, Belgium

* For correspondence. E-mail: maurits.vandegehuchte@ugent.be

Received: 30 October 2013 Returned for revision: 4 December 2013 Accepted: 13 December 2013 Published electronically: 16 February 2014

- **Background** Stem diameter variations are mainly determined by the radial water transport between xylem and storage tissues. This radial transport results from the water potential difference between these tissues, which is influenced by both hydraulic and carbon related processes. Measurements have shown that when subjected to the same environmental conditions, the co-occurring mangrove species *Avicennia marina* and *Rhizophora stylosa* unexpectedly show a totally different pattern in daily stem diameter variation.
- **Methods** Using *in situ* measurements of stem diameter variation, stem water potential and sap flow, a mechanistic flow and storage model based on the cohesion–tension theory was applied to assess the differences in osmotic storage water potential between *Avicennia marina* and *Rhizophora stylosa*.
- **Key results** Both species, subjected to the same environmental conditions, showed a resembling daily pattern in simulated osmotic storage water potential. However, the osmotic storage water potential of *R. stylosa* started to decrease slightly after that of *A. marina* in the morning and increased again slightly later in the evening. This small shift in osmotic storage water potential likely underlaid the marked differences in daily stem diameter variation pattern between the two species.
- **Conclusions** The results show that in addition to environmental dynamics, endogenous changes in the osmotic storage water potential must be taken into account in order to accurately predict stem diameter variations, and hence growth.

Key words: Functional–structural modelling, *Avicennia marina*, *Rhizophora stylosa*, stem diameter variation, dendrometer, osmotic water potential, endogenous control, mangrove, plant water relations, osmotic regulation, growth, mechanistic model, sap flow.

INTRODUCTION

Radial water transport between the xylem conductive elements and the surrounding storage tissues plays a key role in dynamic water transport in plants (e.g. Steppe *et al.*, 2006; Hölttä *et al.*, 2009; De Schepper and Steppe, 2010; De Swaef *et al.*, 2013b). Water in the storage tissues can buffer discrepancies between water demand and supply, avoiding hydraulic failure in the xylem, and allows turgor to build up. This turgor pressure ultimately enables irreversible growth, provided a specific threshold pressure is overcome (Lockhart, 1965). Moreover, radial water transport is indispensable for the functioning of the phloem (De Schepper *et al.*, 2013). To study this radial water transport, stem diameter variation (SDV) measurements have proven to be a powerful tool (e.g. Zweifel *et al.*, 2000, 2001; Peramaki *et al.*, 2001; Fereris and Goldhamer, 2003; Daudet *et al.*, 2005; De Swaef and Steppe, 2010; Betsch *et al.*, 2011; De Schepper *et al.*, 2012). Daily variations in stem diameter are the result of four main processes: (1) contraction and expansion of dead

conducting elements because of the increase and relaxation of internal tensions; (2) reversible shrinking and swelling of living tissues in relation to different levels of tissue hydration; (3) irreversible radial stem growth; and (4) thermal expansion and contraction. Of these processes, reversible shrinking and swelling and irreversible radial stem growth have the most pronounced effects on SDV. Both processes are the result of the actual radial water transport caused by differences in water potential between the xylem and storage tissues (Daudet *et al.*, 2005).

Experimental studies on C3 and C4 plants have shown that stem diameters tend to decrease in the morning and increase in the afternoon, even though differences in the relative shrinking and swelling were noted depending on species, height within the tree and environmental conditions (e.g. Lovdahl and Odin, 1992; Sevanto *et al.*, 2002; Steppe *et al.*, 2008; De Swaef *et al.*, 2009). It has been commonly accepted that this daily pattern is caused by a water potential difference between xylem and storage tissues, originating from daily hydraulic and carbon-related processes within the tree. In the morning, the tension

inside the xylem increases as transpiration starts, lowering the xylem water potential. When this xylem water potential drops below the storage water potential, water transport from the storage tissues to the xylem causes the stem diameter to decrease (Hinckley and Bruckerhoff, 1975). In the afternoon, when the atmospheric water demand decreases, water can again flow back into the storage tissues if the storage water potential is more negative than the rising xylem water potential, resulting in a stem diameter increase (Molz and Klepper, 1973). Even though the daily stem diameter pattern for CAM plants is reversed, with an increase in the morning and a decrease in the evening, it can still be explained by this same principle, because for CAM plants stomata are closed during the day and opened during the night (Matimati et al., 2012). Besides these hydraulic processes, SDV are influenced by plant carbon relations, including processes such as leaf and woody tissue photosynthesis, starch conversion to sugars, respiration, local production and accumulation of osmotic active compounds such as proline, glycinebetaine, mannitol and inorganic ions, and sink and source activity (Sevanto et al., 2003; Hölttä et al., 2006; Naidoo, 2006; De Schepper and Steppe, 2010; Saveyn et al., 2010; Krauss and Ball, 2013; De Swaef et al., 2013a). De Schepper et al. (2010) showed that the timing of stem diameter shrinking was altered during sink activity manipulation while Sevanto et al. (2003) showed that the time lag between xylem and total stem diameter variation was related to photosynthetic carbohydrate assimilation, carbohydrate transport and sink activity. De Swaef et al. (2013b) reported measurements of the morning increase in tomato SDV, which they attributed to the phenomenon of root pressure, whereby active loading of solutes in the root xylem initiates osmotic water uptake (Kramer and Boyer, 1995).

Recently, M. W. Vandegehuchte et al. (unpubl. res.) discovered that, despite thriving in the same environment, two representatives of the two most dominant mangrove genera (Robert et al., 2009), *Avicennia marina* and *Rhizophora stylosa*, both C3 plants, showed opposite daily stem diameter patterns despite similar long-term trends. The aim of the current work was to assess and discuss the influence of the osmotic storage water potential on SDV and the implications for functional modelling. To this end, ecophysiological measurements conducted on *A. marina* and *R. stylosa* were applied in a mechanistic model based on the cohesion–tension theory.

MATERIALS AND METHODS

Field site

Measurements were conducted at the west coast of North Stradbroke Island, Queensland, Australia (27°27.061'S 135°25.806'E), a vegetated coastal sandy mass island. The island is characterized by sandy soils and acidic water bodies intertwined by a complex mix of perched groundwater-fed freshwater lakes, swamps and creeks (Page et al., 2012). On this field site, three full-grown trees of both *Avicennia marina* and *Rhizophora stylosa* were chosen, located in proximity of each other to avoid tidal effects and spatial salinity gradients (Fig. 1, Table 1). The experimental data were gathered during winter, from 12 August to 11 September (day of year [DOY] 225–255) as during this period dry and mild climatic conditions were expected and the effect of rainfall could be excluded.

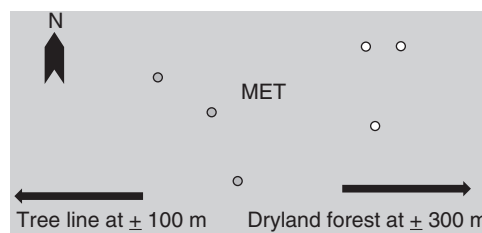


FIG. 1. Schematic of the measured trees at the mangrove site on the west coast of North Stradbroke Island, showing the measured *A. marina* trees (grey circles), the measured *R. stylosa* trees (white circles) and the location of the weather station (MET).

TABLE 1. Diameter at breast height (m) of the measured mangrove trees

Tree					
Av1	Av2	Av3	Rhi1	Rhi2	Rhi3
0-194	0-306	0-181	0-188	0-117	0-172

Environmental conditions

Air temperature, relative humidity, shortwave solar radiation and wind speed were measured every minute and averages recorded every 10 min at 2 m above the soil surface. Rainfall was measured using a tipping-bucket rain gauge and recorded for every tip (HOBO Weather Station, Onset, Cape Cod, MA, USA). Vapour pressure deficit (VPD, kPa) was inferred from measured air temperature (T_{air}) and relative humidity (RH) according to Buck (1981). Soil salinity and water table depth were measured every minute and averages recorded every 10 min from DOY 245 onwards with an *in situ* pressure transducer (Aqua Troll 200, In-Situ, Fort Collins, CO, USA) installed in a piezometer, located close to the weather station at a depth of 0.25 m below the soil surface. Actual measured soil water electrical conductivity (C_a in mS cm^{-1}) was converted to osmotic water potential Ψ_{π} (MPa) based on McIntyre (1980):

$$\Psi_{\pi} = -10^{1.0911 \log(C_a) - 1.46} \quad (1)$$

Plant variables

Each tree was equipped with a dendroband at breast height (DBL60 Logging Band Dendrometer with a resolution of 1 μm , ICT international, Armidale, NSW, Australia), recording stem diameter every 10 min, from which stem diameter variations were derived. Temperature correction of the signals was not deemed necessary as temperature changes have no significant impact on the operation of the DBL60 (ICT international, Armidale, NSW, Australia). Sapflow+ sensors, registering heat velocity every 40 min, were installed at breast height at the south side of each tree (Vandegehuchte and Steppe, 2012). These heat velocities were then converted to sap flow based on wood core measurements of dry wood density and estimations of sapwood depth (Vandegehuchte and Steppe, 2013). Stem water potential was recorded with a stem psychrometer every 10 min (PSY-1 Stem Psychrometer, ICT International, Armidale, NSW, Australia).

Mechanistic stem diameter variation model

The mathematical flow and storage model of [Steppe et al. \(2006\)](#) was applied to enable the assessment of xylem and storage water potential dynamics based on stem sap flow and stem diameter variation measurements. Whereas in the work of [Steppe et al. \(2006\)](#) the aim of the model was to simulate SDV based on measured transpiration, here the objective was to derive the osmotic potential of the stem storage tissues based on the measured sap flow, SDV and soil water potential. In this model, the thickness of the stem storage compartment, encompassing the storage tissues throughout the stem, ΔS (m), was linked to the outer stem diameter D_{out} (m) via an empirical relationship ([Génard et al., 2001](#); [Steppe et al., 2006](#)):

$$\Delta S = a[1 - \exp(-b \times D_{\text{out}})] \quad (2)$$

where a and b are empirical parameters. Based on measurements of bark thickness, as an approximation of ΔS , and stem diameter of the investigated *A. marina* and *R. stylosa* trees, estimates of a and b were obtained, with $a = 0.0035$ m and $b = 18.47$ m⁻¹ for *A. marina* and $a = 0.0153$ m and $b = 10.03$ m⁻¹ for *R. stylosa*, respectively. These parameters were assumed to be constant throughout the measurement period. By subtracting ΔS from the measured input variable D_{out} , the inner diameter of the stem D_{in} could be calculated, as well as the water flow (dV_{st}/dt in m³ s⁻¹) in and out of the stem storage tissue, with l (m) the length of the stem, which was estimated for both species (2 and 4 m for *R. stylosa* and *A. marina*, respectively) (Fig. 2).

$$D_{\text{in}} = D_{\text{out}} - 2\Delta S \quad (3)$$

$$V_{\text{st}} = \pi l(D_{\text{out}}\Delta S - \Delta S^2) \quad (4)$$

The change in V_{st} was directly linked to the storage tissue pressure water potential $\Psi_{\text{p,st}}$, distinguishing between elastic expansion and contraction (if $\Psi_{\text{p,st}} < \Gamma$; eqn 5) or both elastic (el) and plastic (pl) growth (if $\Psi_{\text{p,st}} > \Gamma$; eqn 6) ([Lockhart, 1965](#)):

$$\left(\frac{dV_{\text{st}}}{dt}\right)_{\text{el}} = \frac{V_{\text{st}}}{\varepsilon} \frac{d\Psi_{\text{p,st}}}{dt} \quad \text{for } \Psi_{\text{p,st}} < \Gamma \quad (5)$$

$$\left(\frac{dV_{\text{st}}}{dt}\right)_{\text{el+pl}} = \frac{V_{\text{st}}}{\varepsilon} \frac{d\Psi_{\text{p,st}}}{dt} + V_{\text{st}}\phi(\Psi_{\text{p,st}} - \Gamma) \quad \text{for } \Psi_{\text{p,st}} > \Gamma \quad (6)$$

where ϕ is the extensibility of cell walls in relation to non-reversible dimensional changes (MPa⁻¹ s⁻¹), ε is the bulk elastic modulus of living tissue in relation to reversible dimensional changes (MPa) and Γ is the critical value (in MPa) of the pressure component ($\Psi_{\text{p,st}}$) that must be exceeded to produce irreversible growth in the storage compartment. For this threshold pressure Γ , different values have been observed, ranging from 0.1 to 0.9 MPa ([Green et al., 1971](#); [Green and Cummins, 1974](#); [Hsiao and Xu, 2000](#)). Based on the reasoning of [Génard et al. \(2001\)](#) that Γ has to be higher for stem tissues than for the young tissues or individual cells on which most of the observed values are based, the upper value of 0.9 MPa was chosen for the simulations. As the bulk elastic modulus increases with turgor and cell size ([Tyree and Jarvis, 1982](#); [Dale and](#)

[Sutcliffe, 1986](#)), it was considered proportional to D_{out} and $\Psi_{\text{p,st}}$:

$$\varepsilon = \varepsilon_0 D_{\text{out}} \Psi_{\text{p,st}} \quad (7)$$

where ε_0 is a proportionality constant ([Génard et al., 2001](#); [Steppe et al., 2006](#)).

The variables obtained from this stem diameter variation submodel could then be applied in the water transport submodel (Fig. 2). In this submodel, xylem water potential Ψ_x (MPa) was derived from the root water potential Ψ_r (considered proportional to the soil water potential Ψ_{soil} , applying a proportionality factor, k_{soil}), the measured sap flow F_{sap} (mg s⁻¹) and the xylem resistance to flow R_x (MPa s mg⁻¹). R_x and k_{soil} were calibrated based on stem water potential measurements, applying a 3-day moving window calibration to take temporal variability into account.

The mass flow of water to and from the storage compartment (dW_{st}/dt) was determined from the volumetric flow assuming a constant water density of 1000 kg m⁻³ (ρ_w) and taking into account that only approximately 40 % of the total stem storage volume V_{st} consisted of water ([Steppe et al., 2006](#)):

$$dW_{\text{st}}/dt = 0.4\rho_w dV_{\text{st}}/dt \quad (8)$$

The water potential of the storage tissue could be determined based on the flow to and from this tissue and the exchange resistance R_{st} (MPa s mg⁻¹) between stem storage and stem xylem tissue. The latter was determined based on the assumption that the stem storage and xylem compartments were separated by a virtual membrane with radial hydraulic conductivity L (m MPa⁻¹ s⁻¹; [Steppe et al., 2006](#)).

$$R_{\text{st}} = (\pi D_{\text{in}} L \rho_w)^{-1} \quad (9)$$

$$\Psi_{\text{st}} = \Psi_x - R_{\text{st}} \times dW_{\text{st}}/dt \quad (10)$$

Based on the measured diameter changes, the changes in storage tissue volume could be derived (eqns 3 and 4). From these changes in storage tissue volume, the changes in pressure water potential could be determined based on eqns (5) and (6) (Fig. 2). Knowing the pressure water potential $\Psi_{\text{p,st}}$ of the storage tissue from the stem diameter variation submodel, the osmotic water potential of the storage tissue $\Psi_{\pi,\text{st}}$ could then be derived (Fig. 2).

$$\Psi_{\pi,\text{st}} = \Psi_{\text{st}} - \Psi_{\text{p,st}} \quad (11)$$

From the derived $\Psi_{\pi,\text{st}}$ and V_{st} , a measure for the total amount of osmotically active compounds N_{eq} (mol) in the storage tissue could be derived from the Van't Hoff equation:

$$N_{\text{eq}} = -(\Psi_{\pi,\text{st}}/RT)V_{\text{st}} \quad (12)$$

As no distinction was made between the different compounds or their osmotic activity, N_{eq} is referred to as a number of osmotic equivalents.

While k_{soil} and R_x could be assessed independently through model calibration using the measured xylem water potentials, the parameters L , ϕ and ε_0 remained unknown. For L , values obtained from cells of higher plant tissues between 1.10×10^{-10} and 1.67×10^{-4} m MPa⁻¹ s⁻¹ have been

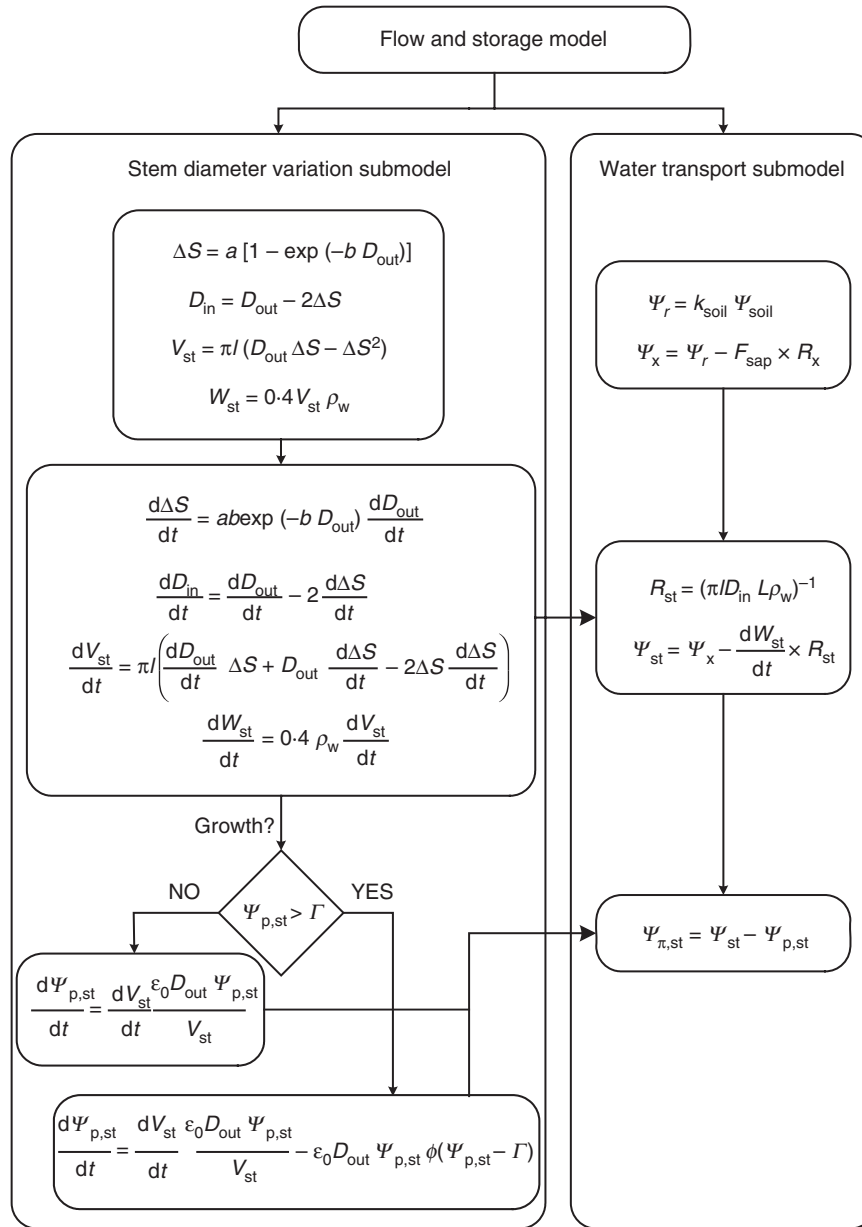


FIG. 2. Schematic overview of the model linking the dynamics of stem diameter variations to stem sap flow and storage. The links between the two submodels mentioned in the text are indicated by arrows. Measurements of D_{out} form the input of the stem diameter submodel whereas the water transport submodel is run on F_{sap} measurements. Symbols are explained in the text.

mentioned (Dainty and Preston, 1963; Dale and Sutcliffe, 1986). For cell wall extensibility ϕ , Hsiao *et al.* (1998) mentioned a range from 8.33×10^{-6} to 5.56×10^{-5} for young plants, although for older tissues the extensibility is likely to be an order of magnitude lower (Génard *et al.*, 2001). The elastic modulus ϵ ranges from 0 to 30 MPa for higher plant tissues (Dainty and Preston, 1963; Dale and Sutcliffe, 1986), allowing a realistic range of 0 to 250 m^{-1} for ϵ_0 based on D_{out} and $\Psi_{p,st}$ values. Table 2 shows the applied parameter values, based on Génard *et al.* (2001) and Stepe *et al.* (2006). To assess the influence of these parameter ranges on the total amount of osmotically active compounds N_{eq} , a Monte Carlo uncertainty analysis was

performed (for procedure see De Pauw *et al.*, 2008b). To this end, a uniform continuous probability distribution function was assigned to each of these parameters using the above-mentioned parameter ranges (Table 2). From these distributions associated with the parameters, 1000 samples were generated using Latin hypercube sampling (e.g. De Pauw *et al.*, 2008b; Helton and Davis, 2003). In a next step, the sampled parameter values were propagated through the model to generate the output uncertainty on the N_{eq} patterns for both species. The upper and lower limits of the uncertainty band were defined as the 95th and 5th percentiles of the resulting output probability distribution constructed from the 1000 different trajectories.

This uncertainty band was used to evaluate actual simulated N_{eq} . Additionally, a sensitivity analysis was conducted according to Brun et al. (2002), Steppe et al. (2006) and De Pauw et al. (2008a) to test the relative impact of the parameters as mentioned in Table 2 on the model output N_{eq} . The centralized relative sensitivity function (s_j) of the model variable y (N_{eq}) towards the parameter θ_j ($L, \epsilon_0, \Gamma, \phi$) was calculated at every time instance k :

$$s_j = \frac{y(\theta_j + \Delta\theta_j) - y(\theta_j - \Delta\theta_j)}{2\Delta\theta_j} \times \frac{\theta_j}{y(\theta_j)} \quad (13)$$

where $\Delta\theta_j$ is taken as 1 % of the parameter value θ_j . As an indication of the relative importance of the parameters on the model output, sensitivity indices (SI) were calculated:

$$SI_j = \sqrt{\frac{1}{K} \sum_{k=1}^K s_{j,k}^2} \quad (14)$$

where j is the j th parameter, k is the time instance within a sensitivity function, K is the number of time instances for a particular sensitivity function and $s_{j,k}^2$ is the squared value of the relative sensitivity (eqn 13) of the variable y to the j th parameter at a certain time instance k .

TABLE 2. Applied model parameters, chosen within the ranges mentioned in literature

Parameter	Value	Uncertainty range
Γ (MPa)	0.9	0.1–0.9
L (m MPa ⁻¹ s ⁻¹)	2.85×10^{-9}	1.1×10^{-10} – 1.67×10^{-4}
ϕ (MPa ⁻¹ s ⁻¹)	2.34×10^{-7}	1×10^{-7} – 5.56×10^{-5}
ϵ_0 (m ⁻¹)	150	0–250

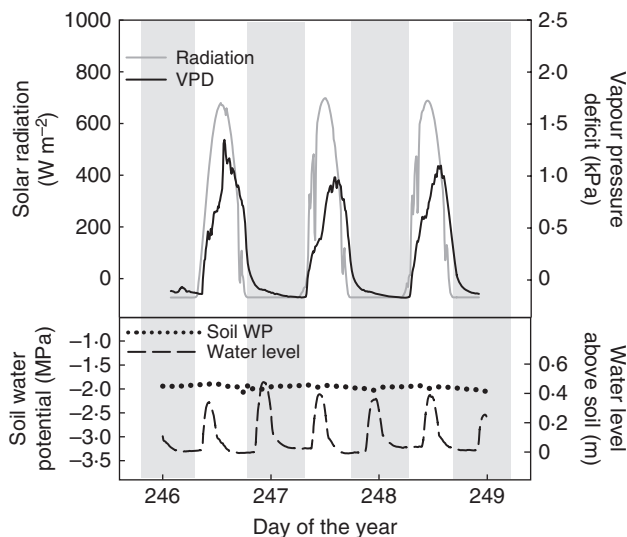


FIG. 3. Typical microclimatic conditions during the dry measurement period. The interval DOY 245–249 is shown as an example.

The model, consisting of a set of algebraic and differential equations, was implemented, simulated and calibrated using the modelling and simulation software package PhytoSim (Phyto-IT BVBA, Mariakerke, Belgium). PhytoSim was also used for the uncertainty and sensitivity analyses.

RESULTS

Given the similar patterns in the ecophysiological variables for the three trees of each species, the average of the three trees per species was considered for further analysis. This way, an investigation of the more general species' water use was conducted rather than focusing on intra-species variability or sensor-specific effects.

In Fig. 3 a typical example of the microclimatic conditions is presented. Throughout the measurement period described in this study, no rain fell and the soil water potential hardly changed, with an average difference between daily minimal and maximal values of 0.10 ± 0.03 MPa. Overall, an average daily soil water potential of -1.99 ± 0.5 MPa was obtained. This value was further applied throughout the model study. Figure 4 indicates that, despite thriving in the same environment and showing

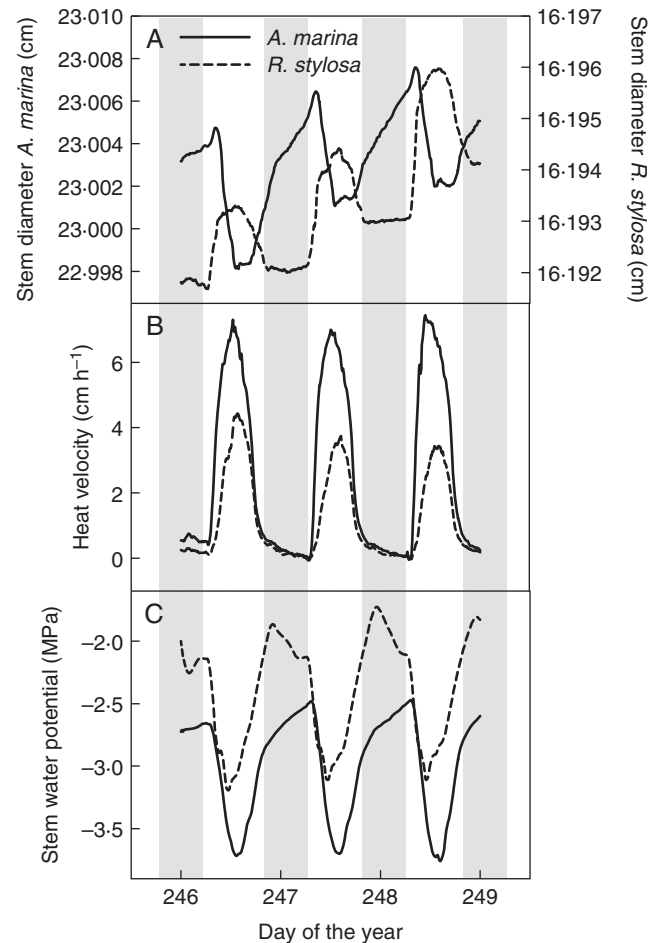


FIG. 4. Measured stem diameter (A), heat velocity as indication of sap flow (B) and stem xylem water potential (C) for *A. marina* and *R. stylosa* for the same time period as shown in Fig. 3. The interval DOY 245–249 is shown as an example; similar patterns were obtained throughout the measurement period.

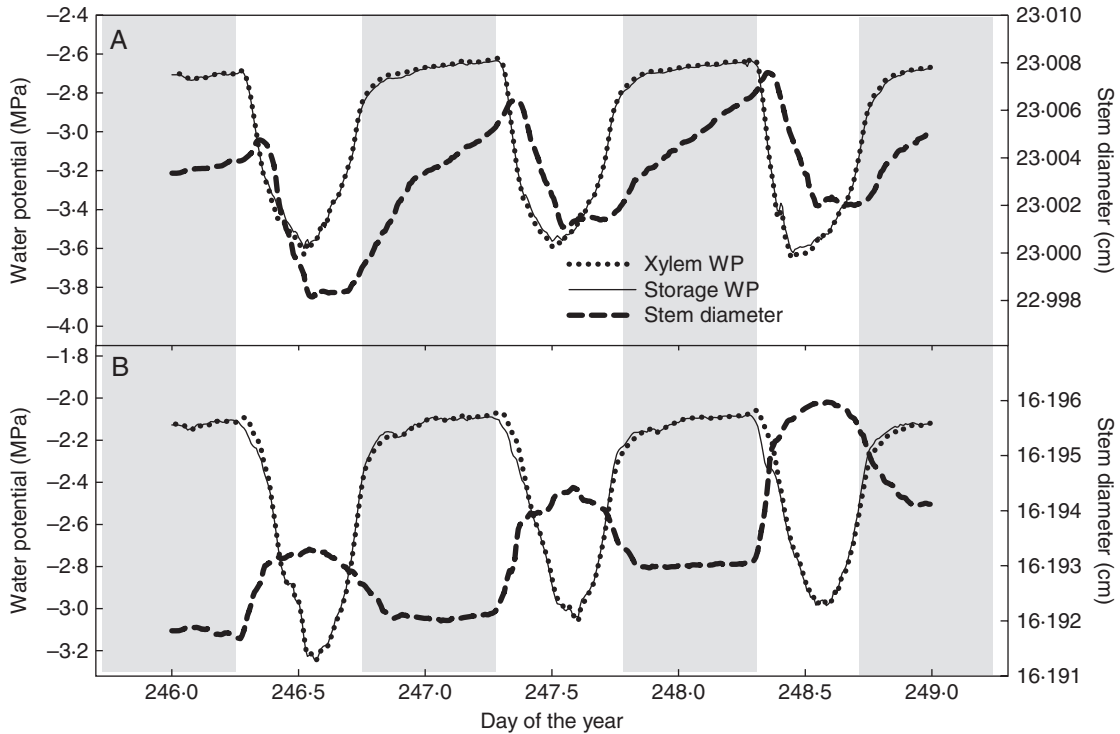


FIG. 5 Model results showing the diameter input and xylem and storage water potential output for *A. marina* (A) and *R. stylosa* (B). The interval DOY 245–249 is shown as an example; similar patterns were obtained throughout the measurement period.

similar dynamics in heat velocity (directly related to sap flow) and xylem water potential pattern, the diurnal SDV pattern was totally different for *A. marina* and *R. stylosa*. While for *A. marina* the stem diameter started to decrease during the morning (often after a short morning increase, as depicted in Fig. 4) and increased again in the evening and during the night, the stem diameter of *R. stylosa* increased during the morning and started to decrease in the afternoon, while remaining more or less constant at night. This pattern was consistent throughout the measurement period. Applying these measured variables to the functional model (Fig. 2), an expected pattern of storage water potential was obtained (Fig. 5). While in *A. marina* the simulated xylem water potential was more negative than the storage water potential during the morning and vice versa during the evening, the opposite happened in *R. stylosa*. The storage pressure potentials obtained were highly linearly correlated to the stem diameter patterns for both species ($R^2 = 0.99$). When the storage osmotic potential and corresponding osmotic equivalents were derived from the storage water potential and the storage pressure potential (eqns 11 and 12), a clear diurnal pattern was obtained for both species (Fig. 6). Note that, for *R. stylosa*, N_{eq} started to increase slightly behind N_{eq} of *A. marina* during the morning. The uncertainty analysis indicated that the N_{eq} patterns obtained remained similar within the possible range of parameter values, as indicated in Table 2 (Fig. 7). Moreover, the effects of ϵ_0 and L on N_{eq} were very limited, as indicated by the low sensitivity indices of 0.004 and 0.0006, respectively. The osmotic equivalent pattern obtained was insensitive to the parameters Γ and ϕ as long as the pressure potential of the osmotic storage tissue was lower than Γ , as then the model only

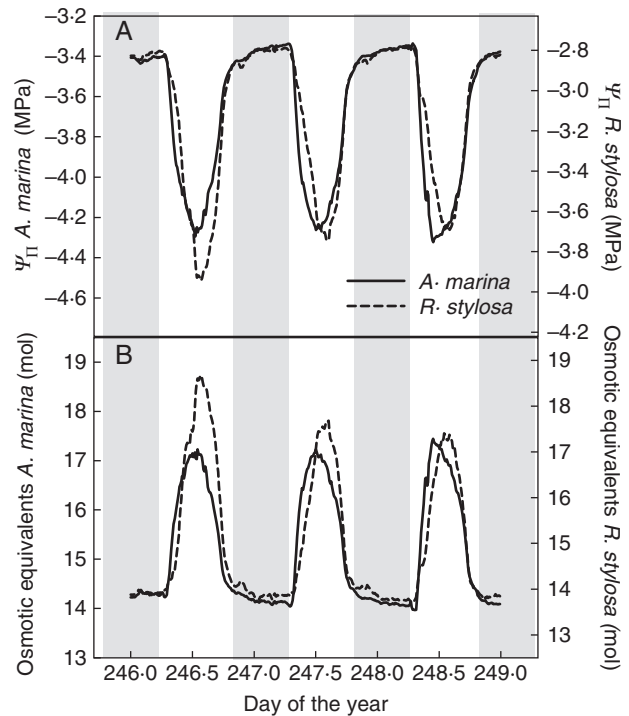


FIG. 6. Modelled osmotic potential of the storage tissue (A) and derived osmotic equivalents of the entire storage pool (B) for *A. marina* and *R. stylosa*. The interval DOY 245–249 is shown as an example; similar patterns were obtained throughout the measurement period.

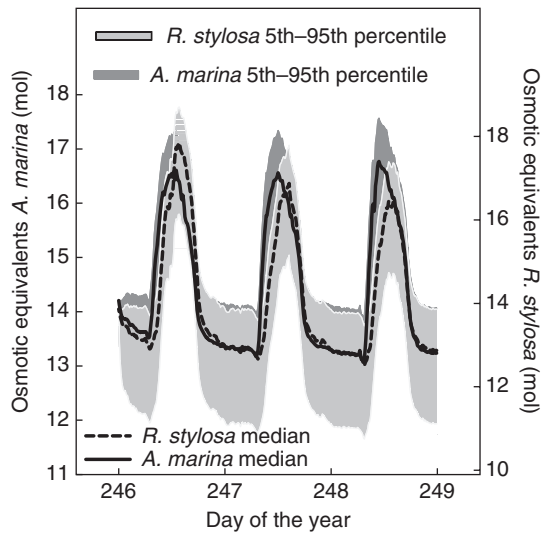


FIG. 7. Median, 5th and 95th percentiles as output of the uncertainty analysis on the osmotic equivalents of the storage pool, taking the possible parameter range as mentioned in Table 2 into account, for *A. marina* and *R. stylosa*. The interval DOY 245–249 is shown as an example; similar patterns were obtained throughout the measurement period.

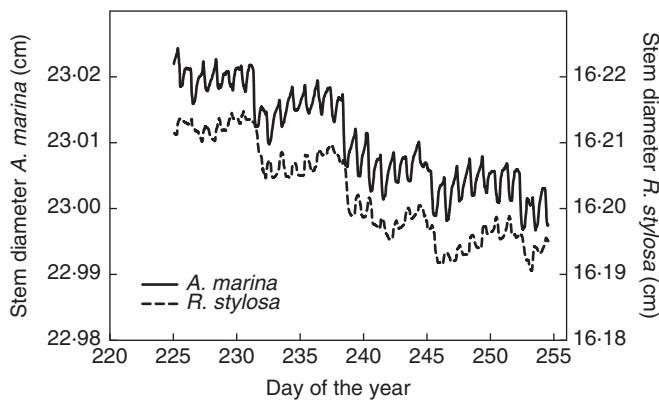


FIG. 8. Average stem diameters for *A. marina* and *R. stylosa* during the dry measurement period. For both mangrove species, a marked decline in stem diameter occurred for DOY 231, 238, 245 and 252.

took elastic growth into account. If, however, Γ was lowered, the N_{eq} patterns became highly sensitive to this parameter (sensitivity index 0.08).

As shown in Fig. 8, the average stem diameter showed an overall decline for both species. Whereas during most days the day-to-day stem diameter changes remained small, on four specific days (DOY 231, 238, 245 and 252) a strong decline in diameter occurred. Days showing a strong decline in diameter were characterized by a lower average relative humidity, resulting in a higher average VPD (M. W. Vandegehuchte *et al.*, unpubl. res.). Nevertheless, the simulated osmotic potential and osmotic equivalent patterns did not differ distinctly from the days without such a marked diameter decline (Fig. 9). Uncertainty analysis across this entire measurement period confirmed that the patterns were not influenced by the choice of parameters within their possible range (data not shown).

DISCUSSION

The observed differences in SDV patterns for *A. marina* and *R. stylosa* point to differences in carbon- and/or ion-related processes, as the measured hydraulic variables for the two species were highly similar (Fig. 4; M. W. Vandegehuchte *et al.*, unpubl. res.). Even though root pressure has been documented to lead to stem diameter increase in the morning (De Swaef *et al.*, 2013b), this phenomenon seems inadequate to explain the *R. stylosa* SDV pattern as the diameter increased continuously when VPD increased and xylem water potential decreased (Figs 4 and 5). Nevertheless, root pressure might have occurred in both mangrove species when VPD was low in the early morning. From our modelling results, it is clear that osmotic adjustment in the storage tissues, whether because of sugar unloading from the phloem (Sevanto *et al.*, 2003, 2011; De Schepper and Steppe, 2010; De Schepper *et al.*, 2013) or local accumulation or synthesis of organic compounds such as proline, glycinebetaine and mannitol and inorganic ions such as sodium and potassium (Popp, 1984a; Popp *et al.*, 1993; Zimmermann *et al.*, 1994; Krauss *et al.*, 2008), contributed to the observed SDV patterns (Figs 6, 7 and 9). The hypothesis that varying osmotic concentrations in the storage tissues influence the SDV dynamics has not only been confirmed in experimental research, but has also been successfully implemented in model studies (Sevanto *et al.*, 2003; Hölttä *et al.*, 2006; De Schepper and Steppe, 2010; De Swaef *et al.*, 2013a). In this study it was remarkable that, for the two co-occurring species, only a slight shift in the pattern of osmotic equivalents (Figs 6 and 9) led to an entirely different SDV pattern (Figs 4A and 8). As for every model, the results obtained were dependent on the estimated parameters. The uncertainty analysis showed that during the night the uncertainty about simulated N_{eq} was larger than that during the day (Fig. 7). Because the uncertainty bands were narrow during the morning increase and evening decrease in N_{eq} , it can be suggested that the morning increase in N_{eq} for *R. stylosa* started slightly after that of *A. marina*. Overall, for both species a clear diurnal pattern was obtained. The uncertainty analysis did not take possible temporal changes of the parameters into account. It has been shown that the radial hydraulic conductivity L may vary depending on the activity and/or abundance of putative aquaporins (Steppe *et al.*, 2012). Nevertheless, in this study the sensitivity analysis indicated that L had little influence on the N_{eq} pattern. Moreover, even on those days when a steep decline in diameter occurred for each species (Fig. 8), the pattern of osmotic equivalents remained largely unaffected (Fig. 9). This raises the question of what the cause of these N_{eq} patterns might be.

In general, the effects of plant carbon status on SDV are somewhat slower than the effects of water status as plants seem to maintain a rather steady supply of carbon to the sinks thanks to temporary storage of carbohydrates under light conditions and remobilization under conditions of low or absent photosynthesis (Geiger *et al.*, 2000; Komor, 2000; De Swaef *et al.*, 2013a). Nevertheless, De Swaef *et al.* (2013a) indicated that the high correspondence between variations in measured photosynthetically active radiation and growth rate of tomato highlighted the effect of varying plant carbon status on SDV. They showed that, besides the instantaneous dynamics of the plant water relations, osmotic variations in the phloem caused by varying soluble carbohydrate content for tomato plants with limited starch reserves could

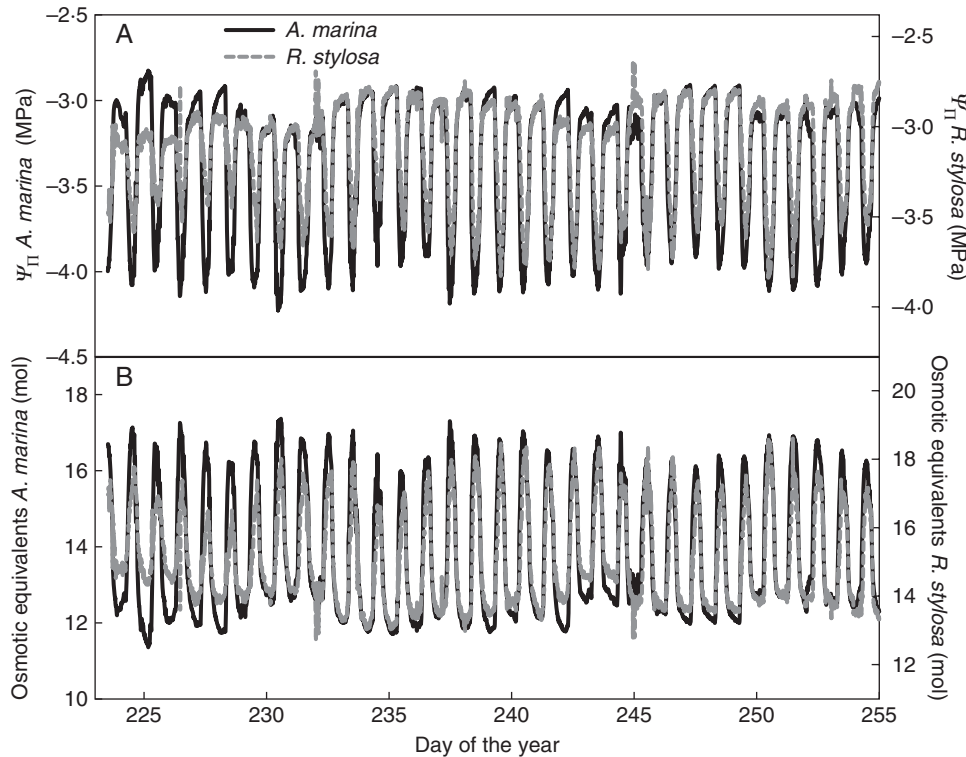


FIG. 9. Modelled osmotic potential of storage tissue (A) and derived osmotic equivalents of the entire storage volume (B) for *A. marina* and *R. stylosa* for the dry measurement period, including days with a typical decline in diameter.

explain the measured SDV. These authors hypothesized that the lower the starch reserve in plants, the more pronounced the influence of carbon status on SDV, which might be an indication of carbon starvation. This fits the expectations of Komor (2000), who stated that the balance between carbon storage and phloem carbon loading is subject to adaptation to meet growth requirements under special circumstances, enabling the modulation of symplastic and apoplastic carbon transport pathways by environmental factors. Thus, carbohydrate transport to and from the phloem may partly explain the N_{eq} patterns as modelled for *A. marina* and *R. stylosa*. As it is clear from the long-term measurements (Fig. 8) that both mangrove species were subjected to stress, the loading of sufficient carbohydrates during the daytime might have been essential to sustain turgor in the phloem tissues and avoid cell lesion. For *R. stylosa*, it even seemed essential to enable growth, as only during the morning increase in N_{eq} was stem diameter able to exceed the maximum diameter observed the previous day. Moreover, it is likely that during the dry measurement period, carbohydrate reserves were limited; following the hypothesis of De Swaef *et al.* (2013a), this could imply that, during more favourable conditions, the N_{eq} patterns might be less pronounced, which could affect the osmotic water potential of the storage tissues and hence the SDV pattern. Long-term measurements during the wet season could confirm this.

Next to carbohydrate loading and unloading, compartmentalization of ions and the formation of low molecular weight carbohydrates as osmotic adjusters might play a role in N_{eq} and SDV dynamics. While these processes have been mainly studied at leaf level (Popp, 1984a, b; Rada *et al.*, 1989; Sobrado, 2005;

Naidoo, 2006), it is not unlikely that they may also affect the storage tissues at stem level. However, to further investigate the cause of the N_{eq} and SDV pattern it would be necessary to sample the storage tissues to analyse their non-structural carbohydrate and ionic composition over time. Additionally, the simultaneous measurement of xylem and over-bark stem diameter variations might provide evidence of the N_{eq} pattern as the lag between these two diameter measurements indicates the transport of carbohydrates and sink activity (Sevanto *et al.*, 2003).

As the model applied in this study did not include detailed structural information, many structural differences between *A. marina* and *R. stylosa* were not directly taken into account. However, these differences likely contributed to the difference in SDV pattern. The leaves of *R. stylosa* are much more succulent and more vertically orientated, which may cause differences in the timing and rate of carbohydrate assimilation and transpiration. Additionally, *A. marina* is characterized by a patchy network of phloem strings throughout the xylem, which has not been shown for *R. stylosa* (Schmitz *et al.*, 2008). Moreover, *A. marina* is considered to be a salt excluder, while *R. stylosa* is known to rely predominantly on salt filtration at root level (Ball, 1988). These differences influence xylem sap salinity, which may affect xylem hydraulic conductivity (Lopez-Portillo *et al.*, 2005). Inclusion of these features in the model might provide new insights into the underlying cause of the differing SDV patterns, but would greatly increase model complexity and require additional measurements (e.g. photosynthesis, respiration, wood anatomical features, leaf angle and xylem sap osmotic concentrations).

Nevertheless, despite the exclusion of this detailed structural information, the mechanistic approach applied here remains valid. The results indicate that both mangrove species are characterized by an endogenous osmotic adaptation that might be a function of environmental stress. The gradual overall decline in stem diameter indicates, however, that this osmotic adaptation was insufficient to avoid long-term overall shrinking, especially during days with a steep decline in diameter. During these days, the decline in xylem water potential was less compensated by osmotic adaptive processes, resulting in higher water loss from the storage tissues in both species. Still, SDV and hence growth for these species are clearly determined by both environmental dynamics and endogenous control mechanisms. This points up the importance of correctly implementing carbon-driven and ionic osmotic adaptations in functional–structural plant models to allow accurate predictions of plant behaviour. Our results indeed show that very small differences in osmotically active compound regulation may have drastic influences on important plant physiological measurement variables such as stem diameter variations. More thorough knowledge of how these features influence stem diameter variations may result in new insights into why species differ in growth patterns and, hence, which strategies are more beneficial, given specific environmental conditions. Moreover, it may allow assessment of the relative importance of endogenous osmotic adaptations, such as carbohydrate loading and unloading, local production and accumulation of osmotically active compounds, and environmental dynamics to long-term growth.

Conclusions

The present research highlights the importance of endogenous osmotic adaptations for SDV and, by extension, radial stem growth, illustrated for the two common mangrove species *A. marina* and *R. stylosa*. Based on ecophysiological measurements and mechanistic modelling, the daily pattern of osmotically active compounds in the storage tissues was unveiled, indicating that only a minor difference in this pattern can cause large differences in daily SDV. Our results stress the importance of correct implementation of endogenous osmotic processes in functional plant models.

ACKNOWLEDGEMENTS

We thank Matthew Hayes, Nina Welti, Stefanie De Groote, Mieke Van Houtte, Michiel Hubeau and Niels De Baerdemaeker for their help during field work. We are also indebted to the Moreton Bay Research Station, University of Queensland, for their technical support. The National Centre for Groundwater Research and Training is a co-funded Centre of Excellence of the Australian Research Council and the National Water Commission. We also thank Philip Deman, Geert Favvyts and Erik Moerman for their technical assistance during the construction of the Sapflow+ sensors. This work was supported by the Fund for Scientific Research–Flanders (FWO) through the PhD grant to M.W.V. and a travel grant allowing the research stay at the University of Queensland. The Commission for Scientific Research (CWO) of Ghent University funded the travel grant of Stefanie De Groote, Mieke Van Houtte, Michiel Hubeau and Niels De Baerdemaeker, which enabled their aid during field work.

LITERATURE CITED

- Ball MC. 1988.** Ecophysiology of mangroves. *Trees: Structure and Function* **2**: 129–142.
- Betsch P, Bonal D, Breda N, et al. 2011.** Drought effects on water relations in beech: the contribution of exchangeable water reservoirs. *Agricultural and Forest Meteorology* **151**: 531–543.
- Brun R, Kühni M, Siegrist H, Gujer W, Reichert P. 2002.** Practical identifiability of ASM2d parameters: systematic selection and tuning of parameter subsets. *Water Research* **36**: 4113–4127.
- Buck AL. 1981.** New equations for computing vapor pressure and enhancement factor. *Journal of Applied Meteorology* **20**: 1527–1532.
- Dainty J. 1963.** Water relations of plant cells. In: Preston RD, ed. *Advanced Botanical Research*. Vol. 1. New York: Academic Press, 279–326.
- Dale JE, Sutcliffe JF. 1986.** Water relations of plant cells. In: Steward FC, ed. *Plant Physiology, Water and Solutes in Plants*. Orlando: Academic Press, 1–48.
- Daudet FA, Ameglio T, Cochard H, Archilla O, Lacoite A. 2005.** Experimental analysis of the role of water and carbon in tree stem diameter variations. *Journal of Experimental Botany* **56**: 135–144.
- Fereris E, Goldhamer DA. 2003.** Suitability of stem diameter variations and water potential as indicators for irrigation scheduling of almond trees. *Journal of Horticultural Science & Biotechnology* **78**: 139–144.
- Geiger DR, Servaites JC, Fuchs MA. 2000.** Role of starch in carbon translocation and partitioning at the plant level. *Australian Journal of Plant Physiology* **27**: 571–582.
- Génard M, Fishman S, Vercambre G, et al. 2001.** A biophysical analysis of stem and root diameter variations in woody plants. *Plant Physiology* **126**: 188–202.
- Green PB, Cummins WR. 1974.** Growth rate and turgor pressure: auxin effect studies with an automated apparatus for single coleoptiles. *Plant Physiology* **54**: 863–869.
- Green PB, Erickson RO, Buggy J. 1971.** Metabolic and physical control of cell elongation rate: in vivo studies in *Nitella*. *Plant Physiology* **47**: 423–430.
- Helton JC, Davis FJ. 2003.** Latin hypercube sampling and the propagation of uncertainty in analyses of complex systems. *Reliability Engineering & System Safety* **81**: 23–69.
- Hinckley TM, Bruckerhoff DN. 1975.** The effects of drought on water relations and stem shrinkage of *Quercus alba*. *Canadian Journal of Botany* **53**: 62–72.
- Hölttä T, Vesala T, Sevanto S, Peramaki M, Nikinmaa E. 2006.** Modeling xylem and phloem water flows in trees according to cohesion theory and Munch hypothesis. *Trees: Structure and Function* **20**: 67–78.
- Hölttä T, Mencuccini M, Nikinmaa E. 2009.** Linking phloem function to structure: analysis with a coupled xylem–phloem transport model. *Journal of Theoretical Biology* **259**: 325–337.
- Hsiao TC, Xu LK. 2000.** Sensitivity of growth of roots versus leaves to water stress: biophysical analysis and relation to water transport. *Journal of Experimental Botany* **51**: 1595–1616.
- Hsiao TC, Frensch J, Rojas-Lara BA. 1998.** The pressure-jump technique shows maize leaf growth to be enhanced by increases in turgor only when water status is not too high. *Plant Cell and Environment* **21**: 33–42.
- Komor E. 2000.** Source physiology and assimilate transport: the interaction of sucrose metabolism, starch storage and phloem export in source leaves and the effects on sugar status in phloem. *Australian Journal of Plant Physiology* **27**: 497–505.
- Kramer PJ, Boyer JS. 1995.** *Water relations of plants and soils*. New York: Academic Press.
- Krauss KW, Ball MC. 2013.** On the halophytic nature of mangroves. *Trees: Structure and Function* **27**: 7–11.
- Krauss KW, Lovelock CE, McKee KL, Lopez-Hoffman L, Ewe SML, Sousa WP. 2008.** Environmental drivers in mangrove establishment and early development: a review. *Aquatic Botany* **89**: 105–127.
- Lockhart JA. 1965.** An analysis of irreversible plant cell elongation. *Journal of Theoretical Biology* **8**: 264–275.
- Lopez-Portillo J, Ewers FW, Angeles G. 2005.** Sap salinity effects on xylem conductivity in two mangrove species. *Plant Cell and Environment* **28**: 1285–1292.
- Lovdahl L, Odin H. 1992.** Diurnal changes in the stem diameter of Norway spruce in relation to relative humidity and air temperature. *Trees: Structure and Function* **6**: 245–251.
- Matimati I, Musil CF, Raitt L, February EC. 2012.** Diurnal stem diameter variations show CAM and C-3 photosynthetic modes and CAM-C-3 switches in

- arid South African succulent shrubs. *Agricultural and Forest Meteorology* **161**: 72–79.
- McIntyre D. 1980.** Basic relationships for salinity evaluation from measurements on soil solution. *Soil Research* **18**: 199–206.
- Molz FJ, Klepper B. 1973.** On the mechanism of water-stress-induced stem deformation. *Agronomy Journal* **65**: 304–306.
- Naidoo G. 2006.** Factors contributing to dwarfing in the mangrove *Avicennia marina*. *Annals of Botany* **97**: 1095–1101.
- Page TJ, Marshall JC, Hughes JM. 2012.** The world in a grain of sand: evolutionarily relevant, small-scale freshwater bioregions on subtropical dune islands. *Freshwater Biology* **57**: 612–627.
- De Pauw DJW, Steppe K, De Baets B. 2008a.** Identifiability analysis and improvement of a tree water flow and storage model. *Mathematical Biosciences* **211**: 314–332.
- De Pauw DJW, Steppe K, De Baets B. 2008b.** Unravelling the output uncertainty of a tree water flow and storage model using several global sensitivity analysis methods. *Biosystems Engineering* **101**: 87–99.
- Peramaki M, Nikinmaa E, Sevanto S, et al. 2001.** Tree stem diameter variations and transpiration in Scots pine: an analysis using a dynamic sap flow model. *Tree Physiology* **21**: 889–897.
- Popp M. 1984a.** Chemical composition of Australian mangroves. 2. Low molecular weight carbohydrates. *Zeitschrift Für Pflanzenphysiologie* **113**: 411–421.
- Popp M. 1984b.** Chemical composition of Australian mangroves. 1. Inorganic ions and organic acids. *Zeitschrift Für Pflanzenphysiologie* **113**: 395–409.
- Popp M, Polania J, Weiper M. 1993.** Physiological adaptations to different salinity levels in mangrove. In: Leith H, Masoom A. eds. *Towards the rational use of high salinity tolerant plants*. New York: Springer.
- Rada F, Goldstein G, Orozco A, Montilla M, Zabala O, Azocar A. 1989.** Osmotic and turgor relations of three mangrove ecosystem species. *Functional Plant Biology* **16**: 477–486.
- Robert EMR, Koedam N, Beeckman H, Schmitz N. 2009.** A safe hydraulic architecture as wood anatomical explanation for the difference in distribution of the mangroves *Avicennia* and *Rhizophora*. *Functional Ecology* **23**: 649–657.
- Saveyn A, Steppe K, Ubierna N, Dawson TE. 2010.** Woody tissue photosynthesis and its contribution to trunk growth and bud development in young plants. *Plant Cell and Environment* **33**: 1949–1958.
- De Schepper V, Steppe K. 2010.** Development and verification of a water and sugar transport model using measured stem diameter variations. *Journal of Experimental Botany* **61**: 2083–2099.
- De Schepper V, Steppe K, Van Labeke M-C, Lemeur R. 2010.** Detailed analysis of double girdling effects on stem diameter variations and sap flow in young oak trees. *Environmental and Experimental Botany* **68**: 149–156.
- De Schepper V, van Dusschoten D, Copini P, Jahnke S, Steppe K. 2012.** MRI links stem water content to stem diameter variations in transpiring trees. *Journal of Experimental Botany* **63**: 2645–2653.
- De Schepper V, De Swaef T, Bauweraerts I, Steppe K. 2013.** Phloem transport: a review of mechanisms and controls. *Journal of Experimental Botany* **64**: 4839–4850.
- Schmitz N, Robert EMR, Verheyden A, Kairo JG, Beeckman H, Koedam N. 2008.** A patchy growth via successive and simultaneous cambia: key to success of the most widespread mangrove species. *Avicennia marina?* *Annals of Botany* **101**: 49–58.
- Sevanto S, Vesala T, Peramaki M, Nikinmaa E. 2002.** Time lags for xylem and stem diameter variations in a Scots pine tree. *Plant Cell and Environment* **25**: 1071–1077.
- Sevanto S, Vesala T, Peramaki M, Nikinmaa E. 2003.** Sugar transport together with environmental conditions controls time lags between xylem and stem diameter changes. *Plant Cell and Environment* **26**: 1257–1265.
- Sevanto S, Holtta T, Holbrook NM. 2011.** Effects of the hydraulic coupling between xylem and phloem on diurnal phloem diameter variation. *Plant Cell and Environment* **34**: 690–703.
- Sobrado MA. 2005.** Leaf characteristics and gas exchange of the mangrove *Laguncularia racemosa* as affected by salinity. *Photosynthetica* **43**: 217–221.
- Steppe K, De Pauw DJW, Lemeur R, Vanrolleghem PA. 2006.** A mathematical model linking tree sap flow dynamics to daily stem diameter fluctuations and radial stem growth. *Tree Physiology* **26**: 257–273.
- Steppe K, De Pauw DJW, Lemeur R. 2008.** A step towards new irrigation scheduling strategies using plant-based measurements and mathematical modelling. *Irrigation Science* **26**: 505–517.
- Steppe K, Cochard H, Lacoite A, Ameglio T. 2012.** Could rapid diameter changes be facilitated by a variable hydraulic conductance? *Plant Cell and Environment* **35**: 150–157.
- De Swaef T, Steppe K. 2010.** Linking stem diameter variations to sap flow, turgor and water potential in tomato. *Functional Plant Biology* **37**: 429–438.
- De Swaef T, Steppe K, Lemeur R. 2009.** Determining reference values for stem water potential and maximum daily trunk shrinkage in young apple trees based on plant responses to water deficit. *Agricultural Water Management* **96**: 541–550.
- De Swaef T, Driever SM, Van Meulebroek L, Vanhaecke L, Marcelis LFM, Steppe K. 2013a.** Understanding the effect of carbon status on stem diameter variations. *Annals of Botany* **111**: 31–46.
- De Swaef T, Hanssens J, Cornelis A, Steppe K. 2013b.** Non-destructive estimation of root pressure using sap flow, stem diameter measurements and mechanistic modelling. *Annals of Botany* **111**: 271–282.
- Tyree MT, Jarvis PG. 1982.** Water in tissues and cells. In: Lange OL, Nobel PS, Osmond CB, Ziegler H. eds. *Physiological plant ecology II*. Berlin: Springer.
- Vandegehuchte MW, Steppe K. 2012.** Sapflow+: a four-needle heat-pulse sap flow sensor enabling nonempirical sap flux density and water content measurements. *New Phytologist* **196**: 306–317.
- Vandegehuchte MW, Steppe K. 2013.** Sap flux density measurement methods: working principles and applicability. *Functional Plant Biology* **40**: 213–223.
- Zimmermann U, Zhu JJ, Meinzer FC, et al. 1994.** High molecular weight organic compounds in the xylem sap of mangroves: implications for long-distance water transport. *Botanica Acta* **107**: 218–229.
- Zweifel R, Item H, Hasler R. 2000.** Stem radius changes and their relation to stored water in stems of young Norway spruce trees. *Trees: Structure and Function* **15**: 50–57.
- Zweifel R, Item H, Hasler R. 2001.** Link between diurnal stem radius changes and tree water relations. *Tree Physiology* **21**: 869–877.